

# Protein Phosphatase 1 Subunit PPP1R14B Stabilizes STMN1 to Promote Progression and Paclitaxel Resistance in Triple-Negative Breast Cancer



Li Liao<sup>1,2,3</sup>, Yin-Ling Zhang<sup>2</sup>, Ling Deng<sup>1</sup>, Chao Chen<sup>4</sup>, Xiao-Yan Ma<sup>4</sup>, Lisa Andriani<sup>4</sup>, Shao-Ying Yang<sup>1</sup>, Shu-Yuan Hu<sup>1</sup>, Fang-Lin Zhang<sup>2</sup>, Zhi-Min Shao<sup>1,2,3,4,5,6</sup>, and Da-Qiang Li<sup>1,2,3,4,5,6</sup>

## ABSTRACT

Triple-negative breast cancer (TNBC) represents the most lethal subtype of breast cancer due to its aggressive clinical features and the lack of effective therapeutic targets. To identify novel approaches for targeting TNBC, we examined the role of protein phosphatases in TNBC progression and chemoresistance. Protein phosphatase 1 regulatory subunit 14B (PPP1R14B), a poorly defined member of the protein phosphatase 1 regulatory subunits, was aberrantly upregulated in TNBC tissues and predicted poor prognosis. PPP1R14B was degraded mainly through the ubiquitin-proteasome pathway. RPS27A recruited deubiquitinase USP9X to deubiquitinate and stabilize PPP1R14B, resulting in overexpression of PPP1R14B in TNBC tissues. Gain- and loss-of-function assays demonstrated that PPP1R14B promoted TNBC cell proliferation, colony formation, migration, invasion, and resistance to paclitaxel *in vitro*. PPP1R14B also induced xenograft tumor growth, lung metastasis, and paclitaxel resistance *in vivo*. Mechanistic investigations revealed that PPP1R14B maintained

phosphorylation and stability of oncoprotein stathmin 1 (STMN1), a microtubule-destabilizing phosphoprotein critically involved in cancer progression and paclitaxel resistance, which was dependent on PP1 catalytic subunits  $\alpha$  and  $\gamma$ . Importantly, the tumor-suppressive effects of PPP1R14B deficiency could be partially rescued by ectopic expression of wild-type but not phosphorylation-deficient STMN1. Moreover, PPP1R14B decreased STMN1-mediated  $\alpha$ -tubulin acetylation, microtubule stability, and promoted cell-cycle progression, leading to resistance of TNBC cells to paclitaxel. Collectively, these findings uncover a functional and mechanistic role of PPP1R14B in TNBC progression and paclitaxel resistance, indicating PPP1R14B is a potential therapeutic target for TNBC.

**Significance:** PPP1R14B upregulation induced by RPS27A/USP9X in TNBC increases STMN1 activity, leading to cancer progression and paclitaxel resistance.

## Introduction

Breast cancer is the most commonly diagnosed malignancy and the leading cause of cancer-related mortality in females worldwide (1). Triple-negative breast cancer (TNBC) is defined by the lack of expression of both estrogen and progesterone receptors and human epidermal growth factor receptor 2 (HER2), accounting for approximately 15% to 20% of all breast cancers. Compared with other subtypes, TNBC represents the most challenging subtype of breast

cancers due to its higher heterogeneity, higher rates of distant metastasis and disease relapse, and the lack of validated therapeutic targets (2). Currently, the backbone of therapy for patients with TNBC is chemotherapy. Especially, paclitaxel, a microtubule-stabilizing agent, is clinically used as a first-line chemotherapy drug for TNBC patients (3). However, a considerable number of TNBC patients develop drug resistance, thus leading to failure of treatment. Therefore, discovering novel therapeutic targets driving TNBC progression and chemoresistance is urgently needed.

Protein phosphatases (PPP) comprise a large family of enzymes that catalyze the dephosphorylation of protein substrates, thereby counterbalancing the action of protein kinases and controlling an enormous variety of cellular functions (4). The PPP superfamily mainly contains PP1, PP2A, PP2B, and PP4-PP7 subfamilies. Among them, PP1 and PP2A are most abundant and contribute to 90% of dephosphorylation reactions in eukaryotes (5). PP1 is a conserved serine/threonine phosphatase, which exists as a heterodimeric complex consisting of one or two of three catalytic subunits (PP1 $\alpha$ , PP1 $\beta$ / $\delta$ , or PP1 $\gamma$ ) and a variable regulatory subunit (6). To date, approximately 200 putative regulatory subunits have been identified, which dictate subcellular localization, activity, and substrate specificity of PP1, thus playing a fundamental role in the regulation of various cell functions and representing promising therapeutic targets (7). For instance, PP1 regulatory subunits 53 (PPP1R53; also known as BRCA1) functions as a tumor suppressor in breast and ovarian cancer. PPP1R105 (also known as Ki67) is a putative biomarker to predict clinical outcome in postmenopausal women with breast cancer (8). In addition, PPP1R15A and PPP1R15B are promising druggable targets in neurodegenerative disease (9). Despite these important observations, the

<sup>1</sup>Fudan University Shanghai Cancer Center and Institutes of Biomedical Sciences, Fudan University, Shanghai, China. <sup>2</sup>Cancer Institute, Shanghai Medical College, Fudan University, Shanghai, China. <sup>3</sup>Department of Oncology, Shanghai Medical College, Fudan University, Shanghai, China. <sup>4</sup>Department of Breast Surgery, Fudan University Shanghai Cancer Center, Fudan University, Shanghai, China. <sup>5</sup>Shanghai Key Laboratory of Breast Cancer, Shanghai Medical College, Fudan University, Shanghai, China. <sup>6</sup>Shanghai Key Laboratory of Radiation Oncology, Shanghai Medical College, Fudan University, Shanghai, China.

L. Liao, Y.-L. Zhang, and L. Deng authors contributed equally to this work.

**Corresponding Author:** Da-Qiang Li, Fudan University Shanghai and Institute of Biomedical Sciences, Fudan University, 270 Dong-An Road, Shanghai, 200032, China. E-mail: daqiangli1974@fudan.edu.cn; Fang-Lin Zhang, E-mail: mzhangfanglin55@sina.com; and Zhi-Min Shao, E-mail: zhimingshao@yahoo.com

Cancer Res 2023;83:471-84

doi: 10.1158/0008-5472.CAN-22-2709

This open access article is distributed under the Creative Commons Attribution-NonCommercial-NoDerivatives 4.0 International (CC BY-NC-ND 4.0) license.

©2022 The Authors; Published by the American Association for Cancer Research

functional and mechanistic roles of other PP1 regulatory subunits in human diseases remain largely unknown.

PP1 regulatory inhibitor subunit 14B (PPP1R14B), a poorly defined member of the PP1 regulatory subunits, is expressed ubiquitously and functions as a potent inhibitor of PP1 (10). Evidence from drosophila studies indicates that PPP1R14B mutation affects the time of egg activation, the completion of meiosis, and embryogenesis (11). Interestingly, dysregulation of PPP1R14B has been observed in several types of human cancer. In this context, it was recently documented that the expression levels of PPP1R14B are significantly higher in ovarian clear cell carcinoma than those in benign endometriosis (12). Bioinformatic analysis of The Cancer Genome Atlas (TCGA) and Gene-Expression Omnibus databases indicates that PPP1R14B is overexpressed in prostate, ovarian, cervical, and endometrial cancers (13–15), and its upregulation correlates with poor prognosis of patients with chronic lymphocytic leukemia (16). However, the biological functions and molecular mechanisms of PPP1R14B in human cancer are largely undefined.

In this study, we provide the first evidence that PPP1R14B was upregulated in TNBC tumors and promoted TNBC progression and paclitaxel resistance. Mechanistical investigations revealed that ribosomal protein S27a (RPS27A) recruited deubiquitinase ubiquitin-specific protease 9X (USP9X) to inhibit ubiquitination and proteasome degradation of PPP1R14B, thus resulting in PPP1R14B accumulation in TNBC tissues. Moreover, PPP1R14B promoted TNBC progression and paclitaxel resistance through, at least in part, enhancing phosphorylation and stability of oncoprotein stathmin 1 (STMN1). In conclusion, these findings reveal a previously unknown role of the RPS27A/USP9X–PPP1R14B–STMN1 signaling axis in TNBC progression and paclitaxel resistance and identify PPP1R14B as a potential therapeutic target for patients with TNBC.

## Materials and Methods

### Cell culture and reagents

The normal human mammary epithelial cell lines (HMEC and MCF10A), human TNBC cell lines (BT549, HCC1806, HCC1937, SUM159, MDA-MB-231, Hs578T), and human embryonic kidney 293T (HEK293T) cell line were obtained from the Cell Bank of Type Culture Collection of the Chinese Academy of Sciences (Shanghai, China) and Fudan University Shanghai Cancer Center (FUSCC). Cells were expanded and frozen immediately into numerous aliquots after arrival. All cell lines were authenticated through short tandem repeat profiling and were used for less than 6 months within 15 to 20 passages. *Mycoplasma* contamination was tested by a PCR-based method as described previously (17). MCF10A and HMEC cells were maintained as described previously (18). Other cell lines were maintained in DMEM (#L110, BasalMedia) supplemented with 10% FBS (#FSP500, ExCell Biol) and 1% penicillin–streptomycin (#S110B, BasalMedia). All cells were cultured in a 5% CO<sub>2</sub> incubator at 37°C. Detailed information of the chemical reagents used in this study is provided in Supplementary Table S1.

### Clinical samples

Quantitative proteomic dataset (TNBC specimens:  $n = 90$ ; adjacent normal specimens:  $n = 72$ ; ref. 19) and RNA-seq dataset (TNBC specimens:  $n = 360$ ; adjacent normal specimens:  $n = 88$ ; ref. 20) were obtained from FUSCC-TNBC Project cohort. All TNBC specimens and corresponding normal breast tissues were obtained from patients who underwent surgery in FUSCC and had not received any treatment

before. The experimental procedures were approved by the Ethics Committee of FUSCC and the written informed consent was obtained from all participants before surgery.

### Cell proliferation and colony formation assays

For drug-sensitivity assays, cells ( $4 \times 10^3$  per well) were seeded in 96-well plates in triplicate overnight and then treated with or without the indicated concentrations of drugs for 96 hours. Cytotoxicity was assessed using the CCK-8 kit (#40203ES92, Yeasen). For cell viability assays, a total of  $1 \times 10^3$  cells were cultured in 96-well plates in triplicate and the absorbance at 450 nm (A450) was determined at the indicated times. For colony formation assays,  $2 \times 10^3$  cells were plated into 6-well plates in triplicate. After 12 to 14 days, the colonies were fixed with methanol and stained with 0.2% crystal violet.

### Cell migration and invasion assays

For cell migration assays,  $4 \times 10^4$  cells resuspended in serum-free medium were plated in the upper chamber without Matrigel (#353097, Corning). For cell invasion assays,  $8 \times 10^4$  cells were resuspended in serum-free medium and seeded in the upper chamber coated with Matrigel (#354480, Corning). Medium containing 10% FBS (800  $\mu$ L) was added to the lower chamber. After incubation for 20 to 24 hours, the cells in the lower chamber were fixed with methanol and stained with 0.2% crystal violet.

### Xenograft mouse models and treatment

All experimental procedures were approved by the Animal Experiments Committee of FUSCC. To assess tumorigenic ability,  $3 \times 10^6$  cells were inoculated into the mammary fat pads of 6-week-old BALB/c female nude mice ( $n = 10$ ). When the average tumor volumes reached 100 mm<sup>3</sup>, DMSO or paclitaxel (10 mg/kg, dissolved in DMSO) was administered by intraperitoneal injection every 2 days and 6 times in total. Tumor sizes were examined every 3 days, and calculated as tumor volumes = (length  $\times$  width<sup>2</sup>)/2. To assess the ability of lung metastasis,  $1 \times 10^6$  cells were inoculated into the caudal vein of 7-week-old BALB/c female nude mice ( $n = 8$ ). Once the nude mice lost 10% of their weight or developed cachexia, mice were sacrificed, and the tumors or lungs were removed.

### DNA plasmids construction and transfection, lentiviral infection, and siRNA transfection

The cDNAs of PPP1R14B, RPS27A, and STMN1 were amplified using the designed primers (Supplementary Table S2). The mutant STMN1 sequence was synthesized by Sangon Biotech. Subsequently, the cDNA sequences were ligated into the pCDH-CMV-MCS-EF1-Puro or pLVX-IRES-NEO lentiviral vectors to generate pCDH-Flag-PPP1R14B, pLVX-HA-RPS27A, pLVX-Flag-STMN1, and pLVX-Flag-STMN1-Mutant (Mut). The construction of USP9X and ubiquitin (Ub) lentiviral vectors (V5-Ub and HA-Ub) has been described previously (21). The specific sequences of shRNA targeting PPP1R14B, RPS27A, and USP9X were obtained from Sigma-Aldrich Advanced Genomics and then cloned into the pLKO.1-TRC lentiviral vector (Supplementary Table S3). After verification by DNA sequencing, the lentivirus was packaged to infect cells as described previously (18, 22). Small interfering RNAs (siRNA) and the corresponding negative control siRNA (siNC) were obtained from RiboBio (Beijing, China). The detailed sequences are provided in Supplementary Table S4. The siRNA transfection was performed using Lipofectamine 2000 transfection reagent (#11668019, Thermo Fisher Scientific).

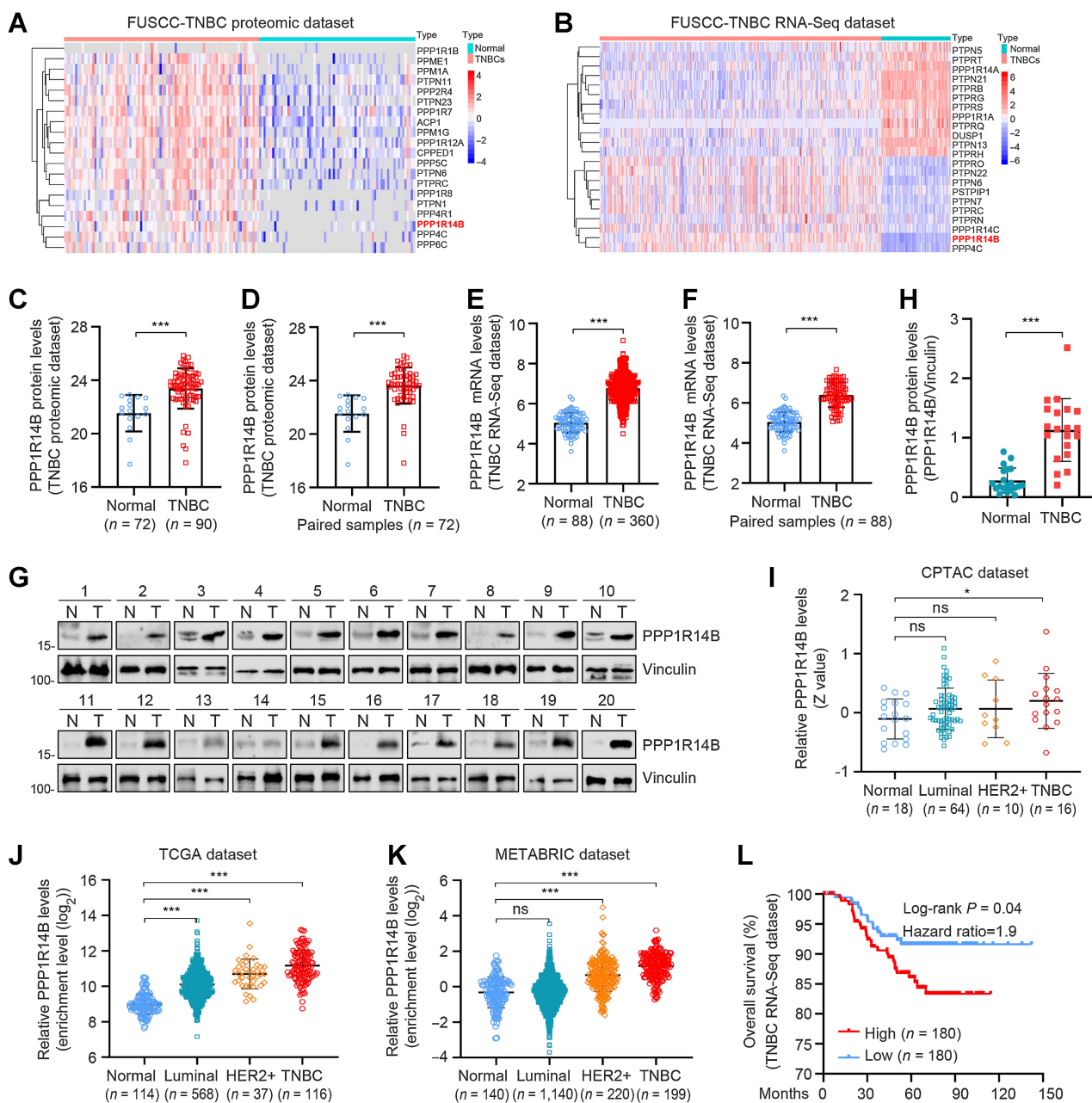


**Figure 1.** PPP1R14B is highly expressed in TNBC and predicts poor OS. **A** and **B**, Dysregulated PPPs in the FUSCC-TNBC proteomic (**A**) and FUSCC-TNBC RNA-seq (**B**) databases, respectively. **C** and **D**, Protein levels of PPP1R14B in 90 TNBC tissues and 72 adjacent normal tissues in the FUSCC-TNBC proteomic database. Y-axis represents the relative abundance of proteins. **E** and **F**, mRNA levels of PPP1R14B in 360 TNBC tissues and 88 adjacent normal tissues in the FUSCC-TNBC RNA-seq database. Y-axis represents the log<sub>2</sub>(FPKM+1). FPKM, fragments per kilobase of transcript per million mapped reads. **G** and **H**, Immunoblotting analysis of PPP1R14B protein expression levels in 20 pairs of TNBC tissues and matched normal breast tissues. The gray intensity was quantified using ImageJ software. Quantitative results of relative PPP1R14B protein expression levels are shown in **H**. N, normal; T, tumor. **I**, Expression levels of PPP1R14B protein in the CPTAC database with different breast cancer subtypes. **J**, Analysis of PPP1R14B mRNA levels in TCGA database with different breast cancer subtypes. **K**, Analysis of PPP1R14B mRNA levels in the METABRIC database with different breast cancer subtypes. **L**, Kaplan-Meier analysis of the OS of TNBC patients with high (n = 180) and low (n = 180) PPP1R14B expression. \*, P < 0.05; \*\*\*, P < 0.001; ns, no significance.

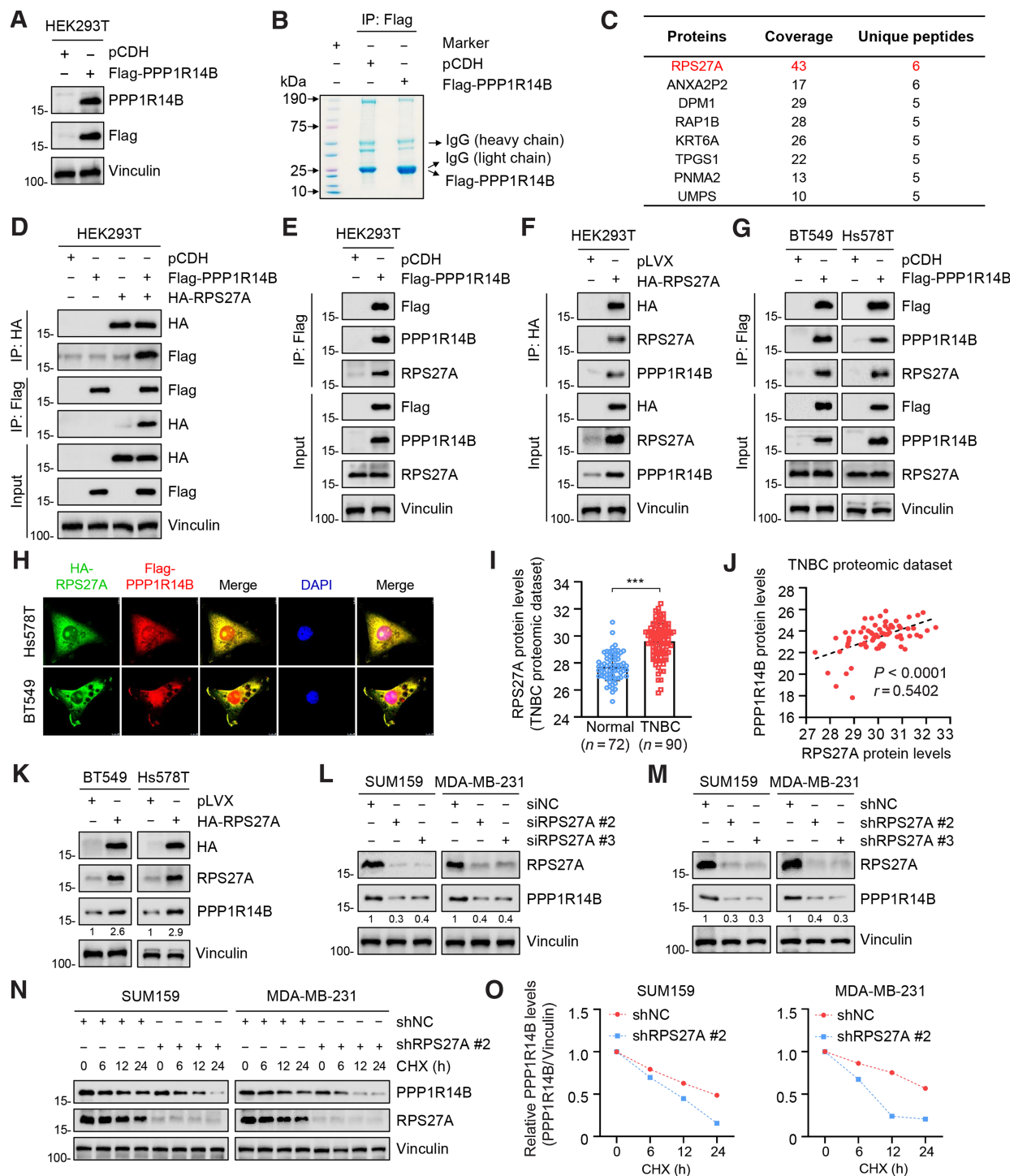


Figure 2.

RPS27A interacts with and stabilizes PPP1R14B in TNBC cells. **A**, Validation of HEK293T cells stably expressing empty vector pCDH and Flag-PPP1R14B by immunoblotting. **B**, HEK293T cells stably expressing empty vector pCDH and Flag-PPP1R14B were subjected to IP assays using anti-Flag affinity gel beads. **C**, The top eight PPP1R14B-interacting proteins according to the number of identified unique peptides. **D** and **E**, IP analysis of the interaction between RPS27A and PPP1R14B in HEK293T cells. HEK293T cells transfected with the indicated expression vectors were subjected to IP assays and followed by immunoblotting with indicated antibodies. **F** and **G**, IP analysis of the interaction between RPS27A and PPP1R14B in TNBC cells. BT549 and Hs578T cell lines stably expressing pCDH and Flag-PPP1R14B were subjected to IP and immunoblotting assays. **H**, Immunofluorescent images showing the colocalization of PPP1R14B and RPS27A in BT549 and Hs578T cell lines stably expressing Flag-PPP1R14B (red) and HA-RPS27A (green) in combination. The nuclear was counterstained with DAPI (blue). **I**, Protein expression levels of RPS27A in 90 TNBC tissues and 72 adjacent normal tissues in the FUSCC-TNBC proteomic database. Y-axis represents the relative abundance of proteins. **J**, Spearman analysis of the correlation of protein levels between PPP1R14B and RPS27A in the FUSCC-TNBC proteomic database. **K**, Immunoblotting assays determining the expression levels of PPP1R14B in BT549 and Hs578T cells stably expressing pLVX and HA-RPS27A. (Continued on the following page.)

### RNA extraction and RT-qPCR

Total RNA was isolated using RNAiso Plus reagent (#9109, Takara), and cDNA was synthesized using HiScript III RT SuperMix reagent (#R323-01, Vazyme). Real-time quantitative PCR (RT-qPCR) was carried out by ChamQ Universal SYBR qPCR Master Mix (#Q711-03, Vazyme). The primers used for RT-qPCR are provided in Supplementary Table S5.

### Immunoblotting assays

For immunoblotting assays, all proteins were extracted using RIPA buffer and quantified using BCA reagent (#20201ES90, Yeasen). Proteins were separated by SDS-PAGE and then transferred onto PVDF membranes (#IPVH00010, Millipore). After blocking in 5% bovine serum albumin (BSA, #36101ES80, Yeasen) and incubating with specific antibodies, the bands were visualized using the enhanced chemiluminescence (ECL) detection kit (#36208ES76, Yeasen), and analyzed by ImageJ software. All antibodies used in this study are provided in Supplementary Table S6.

### Flow cytometry analysis

For cell-cycle analysis, cells were fixed with 70% ethanol overnight. After being washed with PBS, cells were stained with a cell-cycle analysis kit (#40301ES50, Yeasen). To distinguish cells in G<sub>2</sub> or M phase, cells were fixed with 70% ethanol, and then incubated with phospho-histone H3 (Ser10) antibody (p-H3 S10; #53348, CST). After incubation with a FITC-conjugated secondary antibody, flow cytometry analysis was carried out to distinguish p-H3 S10-positive cells.

### Immunofluorescent staining

For immunofluorescent (IF) staining, cells were washed with PBS, fixed with 4% paraformaldehyde, permeabilized with 0.1% Triton X-100 and blocked with 5% BSA. Then, cells were incubated with the corresponding antibodies at 4°C overnight. After being washed with PBS, cells were incubated with the secondary fluorescent antibody at room temperature for 1 hour. Cells were then sealed with Fluoroshield mounting medium with DAPI (#ab104139, Abcam). The Leica SP5 fluorescence confocal microscope was used for imaging.

### Immunoprecipitation assays and proteomics analysis

Immunoprecipitation (IP) assays were carried out as previously described (18). To examine PPP1R14B-interacting proteins, IP coupled with LC-MS/MS analysis was performed as described previously (18, 23). Label-free quantitative proteomic analysis was performed to identify downstream targets of PPP1R14B (Proteomics Center, Institutes of Biomedical Research, Fudan University). The cutoff value of differential expression was set as 1.5-fold change (24). The peptide identification was performed using Proteome Discoverer Software (Thermo Fisher Scientific). The mass spectra were searched against the UniProtKB/Swiss-Prot database restricted to Homo sapiens using Mascot (Matrix Science Ltd.). Protein groups identified with a minimum of two unique peptides and confidence over 95% were considered for further analysis.

### In vivo ubiquitination assays

*In vivo* ubiquitination assays were carried out under denaturing conditions as described previously (18, 22). Briefly, after plasmid transfection, cells were treated with 10 μmol/L MG132 for 6 hours,

and lysed with 100 μL denaturing buffer supplemented with protease and phosphatase inhibitors. Lysates were collected and immediately boiled for 10 minutes. Then, lysates were diluted in 900 μL ice-cold dilution buffer, followed by incubation with immunoblotting assays with the indicated antibodies.

### Statistical analysis

All data are presented as the mean ± standard deviation (SD) from at least three independent experiments. Statistical analysis was carried out using GraphPad (version 8.0.2), R software (version 4.0.3) and SPSS (version 20.0). Statistical analysis of two groups was calculated using two-tailed Student *t* tests or one-way ANOVA. The correlation analysis was calculated using the Spearman test. The survival curve was visualized by the Kaplan–Meier plot method and analyzed by the log-rank test. The growth curves between two groups were compared by two-way ANOVA analysis. *P* < 0.05 was considered as statistically significant (\*, *P* < 0.05; \*\*, *P* < 0.01; \*\*\*, *P* < 0.001; ns, no significance).

### Data and materials availability

The results shown here are based, in part, on data generated by the TCGA (Breast Invasive Carcinoma TCGA PanCancer data), METABRIC (Molecular Taxonomy of Breast Cancer International Consortium, Nature 2012 and Nature Communications 2016), and CPTAC (Clinical Proteomic Tumor Analysis Consortium, Proteogenomic landscape of breast cancer, Cell 2020), and are available in a public repository from the www.cbiportal.org/ websites. All data needed to evaluate the conclusions in the paper are present in the paper and/or Supplementary Materials. Additional data is available upon request from the corresponding author.

## Results

### PPP1R14B is aberrantly expressed in TNBC tissues and predicts poor overall survival of TNBC patients

To identify potential PPP proteins that drive TNBC progression and chemoresistance, we performed integration analyses of our recently published quantitative proteomic dataset (19) and RNA-seq dataset (20) of the FUSCC-TNBC cohort (Supplementary Fig. S1). In the TNBC proteomic dataset, 20 PPP proteins were upregulated in TNBC samples compared with adjacent normal breast tissues (*P* < 0.05; Fig. 1A). In the TNBC RNA-seq dataset, 22 PPP proteins (10 upregulated and 12 downregulated) were dysregulated in TNBC specimens (fold change ≥ 2 and *P* < 0.05; Fig. 1B). Interestingly, we noticed that both protein and mRNA levels of PPP1R14B were elevated in total and paired TNBC specimens (Fig. 1C–F). To demonstrate above results, we collected 20 pairs of primary TNBC specimens and matched adjacent normal tissues to detect the protein levels of PPP1R14B by immunoblotting. As shown in Fig. 1G and H, PPP1R14B was overexpressed in TNBC tissues as compared with normal counterparts.

To further validate our results, we next analyzed the expression levels of PPP1R14B in several public databases, including CPTAC, TCGA, and METABRIC. In agreement with our results, both protein and mRNA levels of PPP1R14B were upregulated in TNBC tissues relative to normal tissues, and its expression levels were higher in TNBC than luminal and HER2-positive subtypes of breast cancer (Fig. 1I–K). Moreover, Kaplan–Meier survival analysis showed that

(Continued.) L and M, Immunoblotting assays assessing the expression levels of PPP1R14B in SUM159 and MDA-MB-231 cells with RPS27A knockdown using siRNA (L) and lentiviral infection (M) targeting RPS27A, respectively. N and O, Immunoblotting assays demonstrating the expression levels of PPP1R14B in SUM159 and MDA-MB-231 cells expressing shNC and shRPS27A (#2) treated with DMSO or 100 μg/mL CHX for the indicated times (N). Quantitative results of relative PPP1R14B protein levels (PPP1R14B/Vinculin) analyzed by ImageJ are shown in O.

PPP1R14B upregulation was associated with poor overall survival (OS) of TNBC patients (Fig. 1L). Collectively, these results suggest that PPP1R14B is upregulated in TNBC and predicts poor prognosis of TNBC patients.

#### RPS27A interacts with and stabilizes PPP1R14B in TNBC cells

To address the molecular mechanism underlying upregulation of PPP1R14B in TNBC tissues, we performed IP assays using anti-Flag beads (Fig. 2A and B), followed by LC-MS/MS analysis to identify PPP1R14B-interacting proteins. By this approach, total 164 proteins that specifically interacted with Flag-PPP1R14B were identified according to the cutoff value of identified unique peptide number over two and confidence over 95%. The top eight PPP1R14B-interacting proteins are listed in Fig. 2C based on the number of identified unique peptides. Ribosomal protein S27a (RPS27A), the top one PPP1R14B-interacting protein, was selected for further validation.

RPS27A is a ubiquitin C-terminal extension protein and regulates ribosome biogenesis, protein posttranslational modification and stability (25). Reciprocal IP assays demonstrated that RPS27A indeed interacted with PPP1R14B in multiple cell lines (Figs. 2D–G). Immunofluorescent staining revealed that PPP1R14B partially colocalized with RPS27A in both BT549 and Hs578T cells (Fig. 2H, yellow color in merge images). In addition, we observed that RPS27A was upregulated in TNBC tissues compared with corresponding normal tissues at both protein and mRNA levels (Figs. 2I; Supplementary Fig. S2A). Spearman analysis revealed that the expression levels of RPS27A were positively correlated with those of PPP1R14B at protein but not mRNA levels (Fig. 2J; Supplementary Fig. S2B).

We next determine whether there is a regulatory relationship between RPS27A and PPP1R14B. As shown in Fig. 2K, ectopic expression of HA-RPS27A resulted in an increase in PPP1R14B protein levels. Conversely, knockdown of RPS27A using siRNAs (Fig. 2L; Supplementary Fig. S2C) or shRNAs (Fig. 2M) reduced PPP1R14B protein levels. However, depletion or overexpression of RPS27A did not significantly affect the mRNA levels of PPP1R14B (Supplementary Fig. S2D and S2E), suggesting that RPS27A regulates PPP1R14B expression at the posttranscriptional level. In addition, knockdown or overexpression of PPP1R14B did not significantly affect RPS27A expression levels (Fig. 2G; Supplementary Fig. S2F). As RPS27A has the potential to regulate the stability of its interacting proteins (25), we then treated cells with protein synthesis inhibitor cycloheximide (CHX) to determine the impact of RPS27A on PPP1R14B stability. As expected, the half-life of PPP1R14B protein was substantially shorter in RPS27A-depleted cells (Fig. 2N and O). Thus, these data demonstrate that RPS27A interacts with and stabilizes PPP1R14B in TNBC cells.

#### PPP1R14B is degraded mainly through the ubiquitin–proteasome pathway

The ubiquitin–proteasome system and the autophagy–lysosome system are two main pathways for protein degradation in eukaryotes. To explore the mechanism of PPP1R14B degradation, cells were treated with autophagy inhibitors bafilomycin A1 (Baf-A1) and proteasome inhibitor MG132 for the indicated times, respectively. Immunoblotting analysis showed that treatment with Baf-A1 did not alter PPP1R14B protein levels (Supplementary Fig. S3A). SQSTM1, a known substrate of the autophagy–lysosome system, was used as a positive control. In contrast, incubation with MG132 resulted in an

obvious accumulation of PPP1R14B and CDKN1A (positive control) in four TNBC cell lines in a time-dependent manner (Fig. 3A). Moreover, RPS27A knockdown significantly reduced PPP1R14B protein levels, which could be restored after treatment with MG132 (Fig. 3B). Ubiquitination assays also demonstrated that ectopic expression of HA-RPS27A decreased, whereas knockdown of RPS27A increased, the ubiquitination levels of PPP1R14B (Fig. 3C and D). These results collectively suggest that PPP1R14B is degraded mainly through the ubiquitin–proteasome but not the autophagy–lysosome pathway.

#### RPS27A recruits USP9X to block ubiquitination-dependent proteasome degradation of PPP1R14B

As RPS27A is not a putative deubiquitinating enzyme (DUB), we predicted that RPS27A might act as an adaptor to recruit DUBs to deubiquitinate PPP1R14B. We examined the list of PPP1R14B-interacting proteins and identified five DUBs, including USP9X, USP7, USP10, OTUB1, and USP5 (Supplementary Fig. S3B). As shown in Figs. 3E and Supplementary Fig. S3C, both protein and mRNA levels of USP9X were upregulated in TNBC tissues compared with normal tissues. Spearman analysis revealed that USP9X was positively correlated with PPP1R14B at protein but not mRNA level (Fig. 3F and G). The expression levels of the other three DUBs in TNBC tissues and their correlation with PPP1R14B were presented in Supplementary Fig. S3D–S3I. In light of the strongest correlation between PPP1R14B and USP9X as well as the priority ranking of USP9X according to the identified peptide score by LC-MS analysis, USP9X was selected for further verification.

Reciprocal IP assays revealed that PPP1R14B interacted with endogenous USP9X and RPS27A (Supplementary Fig. S3J). Knockdown of USP9X downregulated the protein levels of PPP1R14B but not RPS27A (Fig. 3H). However, knockdown of PPP1R14B did not alter USP9X levels (Supplementary Fig. S3K). Moreover, ectopic expression of USP9X indeed reduced the ubiquitination levels of PPP1R14B, whereas this effect was rescued after RPS27A knockdown (Fig. 3I). Reciprocal IP assays revealed that knockdown of RPS27A impaired the interaction between USP9X and PPP1R14B, suggesting that RPS27A may act as an adaptor to recruit USP9X to deubiquitinate PPP1R14B (Fig. 3J and K). Together, these results indicate that RPS27A recruits USP9X to block the ubiquitination-dependent proteasome degradation of PPP1R14B, thus resulting in the overexpression of PPP1R14B in TNBC tissues.

#### PPP1R14B promotes TNBC cell proliferation and colony formation *in vitro* and xenograft tumor growth *in vivo*

To explore the biological functions of PPP1R14B in TNBC progression, we first examined the protein levels of PPP1R14B in six TNBC cell lines and two normal HMEC lines by immunoblotting. Results showed that PPP1R14B was upregulated in TNBC cell lines relative to normal cell lines (Fig. 4A). According to the expression levels of PPP1R14B in these cells, we next stably overexpressed Flag-PPP1R14B in BT549 and Hs578T cells and knocked down endogenous PPP1R14B in SUM159 and MDA-MB-231 cells, respectively. The expression status of PPP1R14B in resultant cell lines was validated by immunoblotting (Fig. 4B and C). CCK-8 and colony formation assays demonstrated that ectopic expression of PPP1R14B promoted cell proliferation (Fig. 4D) and colony formation capability (Fig. 4E and F), whereas opposite results were obtained following PPP1R14B knockdown (Fig. 4G–J). In xenograft tumor mouse models, knockdown of PPP1R14B also

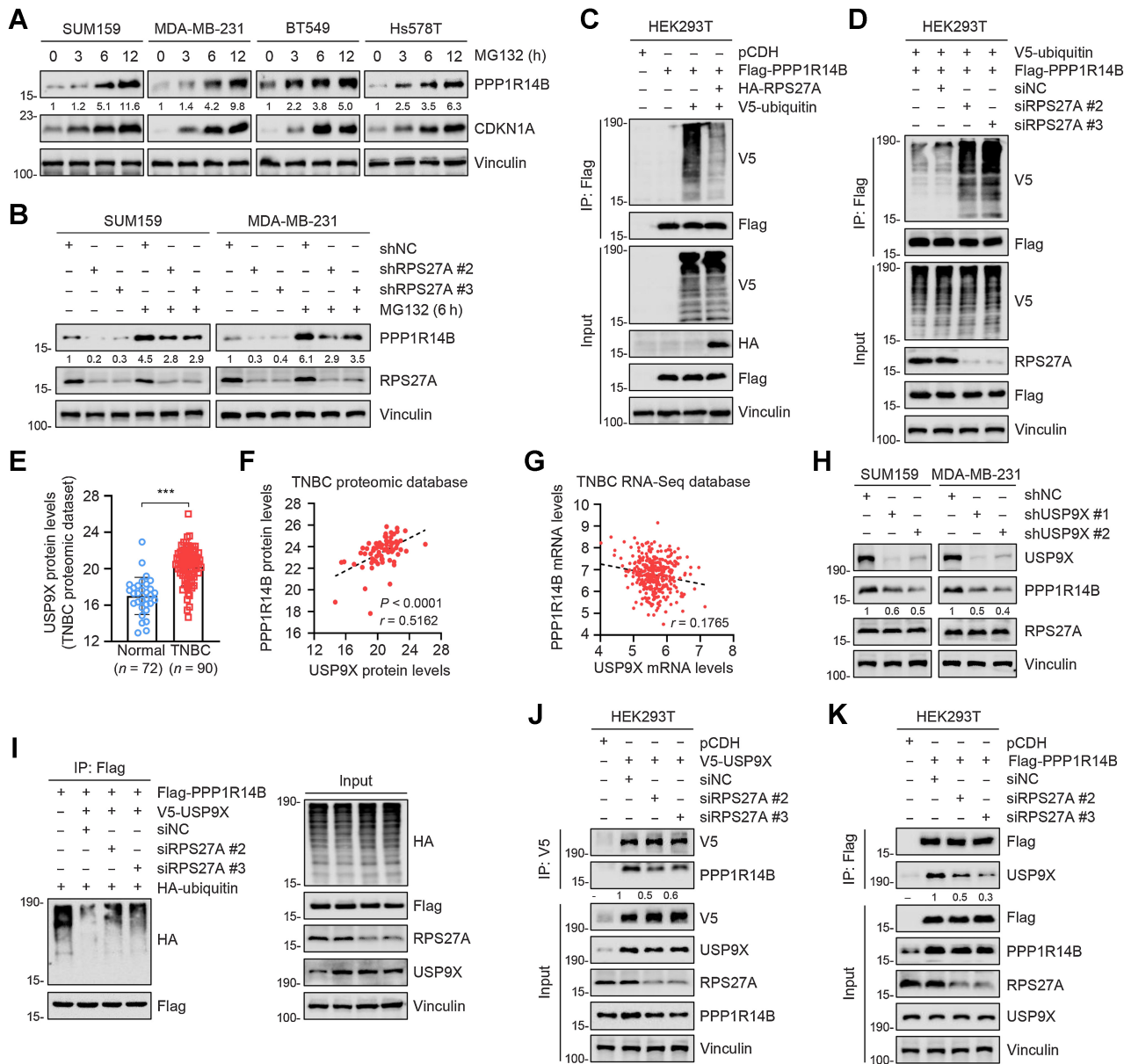


**Figure 3.** RPS27A recruits USP9X to block ubiquitination-dependent proteasome degradation of PPP1R14B. **A**, Immunoblotting assays showing the expression levels of PPP1R14B in TNBC cells treated with DMSO or 10  $\mu$ mol/L MG132. CDKN1A was used as a positive control. **B**, Immunoblotting assays examining the expression levels of PPP1R14B in SUM159 and MDA-MB-231 cells expressing shNC and shRPS27A (#2 and #3) treated with DMSO or 10  $\mu$ mol/L MG132 for 6 hours. **C** and **D**, Immunoblotting assays assessing the expression levels of PPP1R14B ubiquitination in HEK293T cell lines transfected with HA-RPS27A (**C**) or siRNAs targeting RPS27A (#2 and #3; **D**). After transfection with the indicated plasmids for 48 hours, the cells were treated with 10  $\mu$ mol/L MG132 for 6 hours and then subjected to IP and subsequent immunoblotting analysis. **E**, Protein expression levels of USP9X in 90 TNBC tissues and 72 adjacent normal tissues in the FUSCC-TNBC proteomic database. **F** and **G**, Spearman analysis of the correlation of the protein (**F**) and mRNA (**G**) levels between PPP1R14B with USP9X. **H**, Immunoblotting assays determining the expression levels of PPP1R14B and RPS27A in SUM159 and MDA-MB-231 cells stably expressing shNC and shUSP9X (#1 and #2). **I**, Immunoblotting assays demonstrating the expression levels of PPP1R14B ubiquitination in HEK293T cell lines transfected with the indicated plasmids. After transfection for 48 hours, the cells were treated with 10  $\mu$ mol/L MG132 for 6 hours and then subjected to IP and subsequent immunoblotting analysis. **J** and **K**, Immunoblotting assays investigating the expression levels of the binding proteins PPP1R14B (**J**) and USP9X (**K**) in HEK293T cell lines transfected with the indicated plasmids. \*\*\*,  $P < 0.001$ .

significantly reduced tumor weight and volume (Fig. 4K–M). The expression levels of PPP1R14B in xenograft tumors are shown in Supplementary Fig. S4A. Together, these results suggest PPP1R14B promotes TNBC cell proliferation and colony formation *in vitro* as well as xenograft tumor growth *in vivo*.

**PPP1R14B promotes TNBC cell migration and invasion *in vitro* and lung metastatic potential *in vivo***

Given the highly invasive and metastatic potential of TNBC cells, we next examined whether PPP1R14B could affect the migratory and invasive capacities of TNBC cells. Transwell assays showed

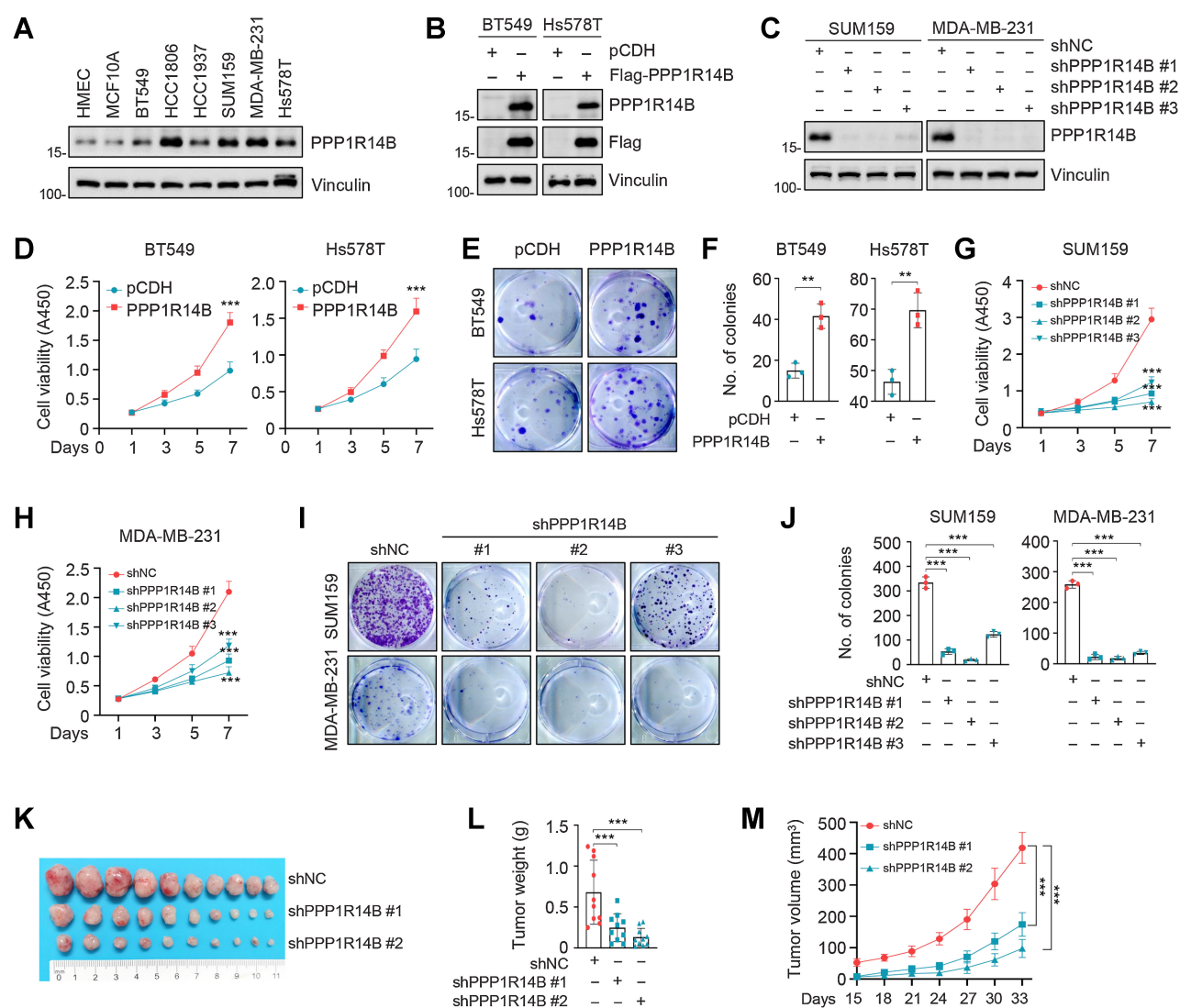


**Figure 4.** PPP1R14B promotes TNBC cell proliferation and colony formation *in vitro* and xenograft tumor growth *in vivo*. **A**, Immunoblotting analysis of PPP1R14B protein expression levels in two normal HMEC lines and six TNBC cell lines. **B**, Expression validation of BT549 and Hs578T cells stably expressing empty vector pCDH and Flag-PPP1R14B after lentiviral infection. **C**, Verification of knockdown efficiency in SUM159 and MDA-MB-231 cells stably expressing empty vector shNC and shPPP1R14B (#1, #2, and #3) by immunoblotting. **D-F**, BT549 and Hs578T cells stably expressing pCDH and Flag-PPP1R14B were subjected to CCK-8 (**D**) and colony formation assays (**E** and **F**). Representative images of the survival colonies (**E**) and corresponding quantitative results (**F**) are shown. **G-J**, SUM159 and MDA-MB-231 cells stably expressing shNC and shPPP1R14B (#1, #2, and #3) were subjected to CCK-8 (**G** and **H**) and colony formation assays (**I** and **J**). Representative images of the survival colonies (**I**) and corresponding quantitative results (**J**) are shown. **K-M**, MDA-MB-231 cells stably expressing shNC and shPPP1R14B (#1 and #2) were inoculated into mammary fat pad of 6-week-old BALB/c female nude mice ( $n = 10$ ). After 33 days of injection, mice were sacrificed and xenograft tumors were removed. Representative tumor images (**K**), tumor weight (**L**), and tumor volume (**M**) are shown. \*\*,  $P < 0.01$ ; \*\*\*,  $P < 0.001$ .

that ectopic expression of PPP1R14B enhanced migratory and invasive potential of BT549 and Hs578T cells (Fig. 5A–D), whereas knockdown of PPP1R14B impaired these abilities (Fig. 5E–H). To validate these results, the tail-vein injection model was used to examine the effects of PPP1R14B on TNBC metastasis *in vivo*. As expected, there were fewer metastatic nodes and lower lung metastasis incidence of mice bearing tumors with PPP1R14B knockdown ( $n = 8$ ) than those in control mice ( $n = 8$ ; Fig. 5I and J; Supplementary Fig. S4B–S4D). Collectively, these results suggest that PPP1R14B promotes TNBC cell migration and invasion *in vitro* and lung metastasis *in vivo*.

#### PPP1R14B regulates phosphorylation and stability of STMN1 partially depending on PP1 catalytic subunits $\alpha$ and $\gamma$

To investigate the downstream targets regulated by PPP1R14B, label-free-based quantitative proteomic assays was performed (Fig. 6A). Results showed that 153 proteins were downregulated and 375 proteins were upregulated after PPP1R14B knockdown (Fig. 6B). GO-BP, GO-MF, and KEGG pathway analyses revealed that these differentially expressed proteins were mainly involved in cell–cell adhesion, cell proliferation, and protein processing in the endoplasmic reticulum (Supplementary Fig. S5A–S5C). According to the cutoff value of 1.5-fold change, the top 10 downregulated proteins following

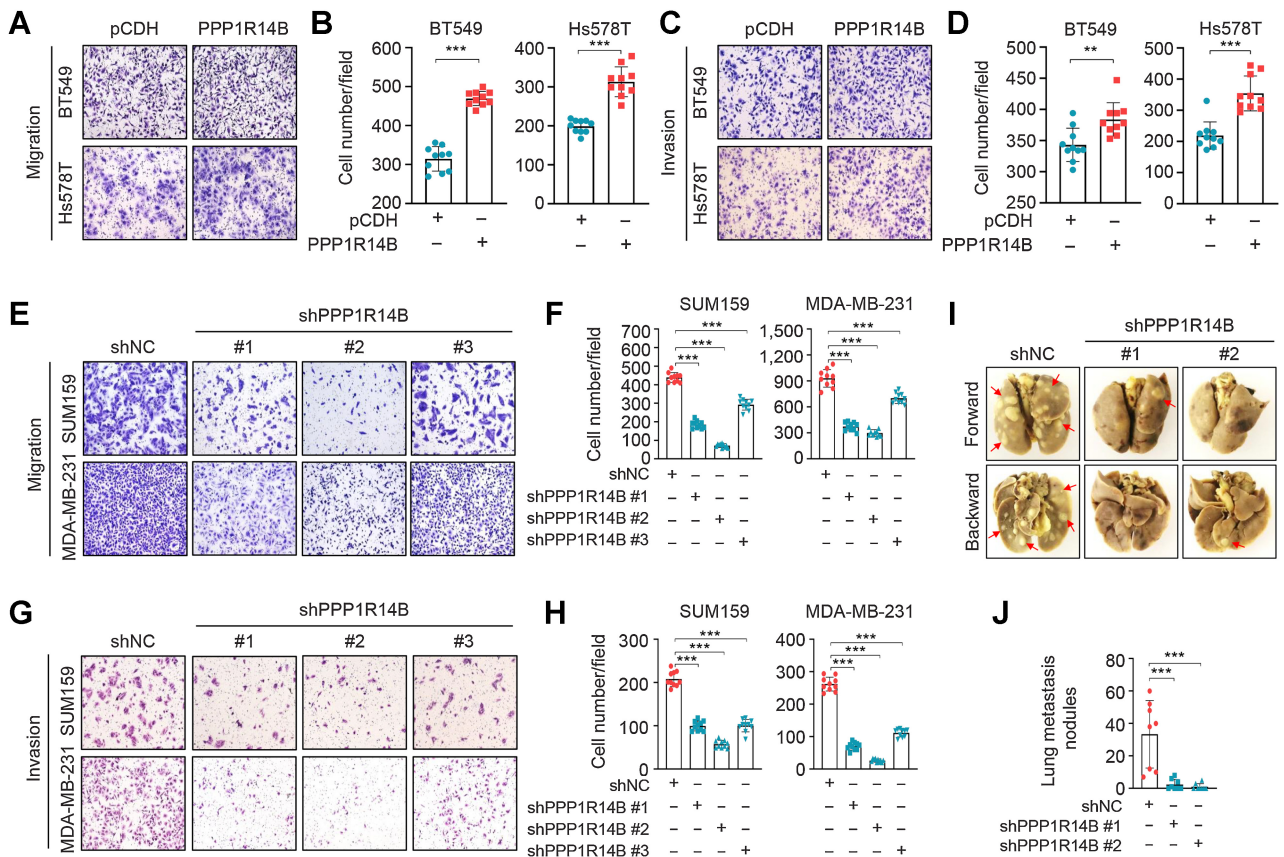


**Figure 5.** PPP1R14B promotes TNBC cell migration and invasion *in vitro* and lung metastatic potential *in vivo*. **A-D**, BT549 and Hs578T cells stably expressing pCDH and Flag-PPP1R14B were subjected to Transwell migration (**A** and **B**) and invasion (**C** and **D**) assays. Representative images of migrated and invaded cells are shown in **A** and **C**, and the corresponding quantitative results are shown in **B** and **D**. **E-H**, SUM159 and MDA-MB-231 cells stably expressing shNC and shPPP1R14B (#1, #2, and #3) were subjected to Transwell migration (**E** and **F**) and invasion (**G** and **H**) assays. Representative images of migrated and invaded cells are shown in **E** and **G**, and corresponding quantitative results are shown in **F** and **H**. **I** and **J**, MDA-MB-231 cells stably expressing shNC and shPPP1R14B (#1 and #2) were injected into the tail vein of 7-week-old BALB/c female nude mice ( $n = 8$ ). Representative images of lung metastasis (**I**) and corresponding quantitative results of metastatic lung nodules (**J**) are shown. \*\*,  $P < 0.01$ ; \*\*\*,  $P < 0.001$ .

PPP1R14B knockdown are presented in **Fig. 6C**. Given that the role of RIN1 in human cancer is ambiguous (26) and there was no correlation of RIN1 expression levels with PPP1R14B in TNBC tissues (Supplementary Fig. S5D and S5H), the top three proteins, including stathmin 1 (STMN1), MAPK3 (ERK1), and MAPK1 (ERK2), were selected for further verification.

Based on the FUSCC-TNBC RNA-seq database, the expression levels of these three molecules in TNBC and corresponding normal tissues are shown in Supplementary Fig. S5E–S5G. In addition, Spearman analysis showed that the correlation between PPP1R14B and STMN1, ERK1, and ERK2 was not significant at the mRNA level (Supplementary Fig. S5I–S5K). In contrast, in the FUSCC-TNBC proteomics database, the protein expression levels of STMN1, ERK1, and ERK2 were all upregulated in TNBC tissues and strongly correlated with those of PPP1R14B (**Fig. 6D** and **E**).

As PPP1R14B is a PP1 regulatory subunit, we predicted that it may have a role in regulating phosphorylation status of its downstream molecules. It has been reported that STMN1 has four serine (S) phosphorylation sites, including S16, S25, S38, and S63 (27). Immunoblotting assays verified that PPP1R14B indeed positively regulated the expression levels of total and phosphorylated STMN1 and ERK1/2 (**Fig. 6F** and **G**). Moreover, we found that knockdown of RPS27A led to

a decrease in the levels of total and phosphorylated STMN1 at S16, S25, S38, and S63, whereas these effects were reversed when PPP1R14B was ectopically expressed (**Fig. 6H**).

As reported previously, there are three PP1 catalytic subunits, including PP1 $\alpha$ , PP1 $\beta$ , and PP1 $\gamma$ . IP assays demonstrated that PPP1R14B interacted with PP1 $\alpha$  and PP1 $\gamma$ , but not PP1 $\beta$ , to form a PP1 complex holoenzyme (Supplementary Fig. S5L). To explore whether PPP1R14B mediated STMN1 phosphorylation depends on PP1 $\alpha$  and PP1 $\gamma$ , two independent siRNAs were used to knock down PP1 $\alpha$  and PP1 $\gamma$ , respectively (Supplementary Fig. S5M). Interestingly, PPP1R14B-mediated STMN1 phosphorylation was partially impaired after knockdown of PP1 $\alpha$  and PP1 $\gamma$  alone or in combination (**Fig. 6I**). Collectively, PPP1R14B regulates STMN1 phosphorylation and stability partially in the form of PP1 holoenzyme.

**PPP1R14B accelerates TNBC progression via STMN1 phosphorylation**

To explore whether PPP1R14B accelerates TNBC progression through regulating STMN1 phosphorylation, we generated stable cell lines expressing wild-type STMN1 (STMN1-WT) and alanine-substituted STMN1 comutants (S16A, S25A, S38A, and S63A; thereafter termed STMN1-Mut; Supplementary Fig. S6A and S6B). CHX-

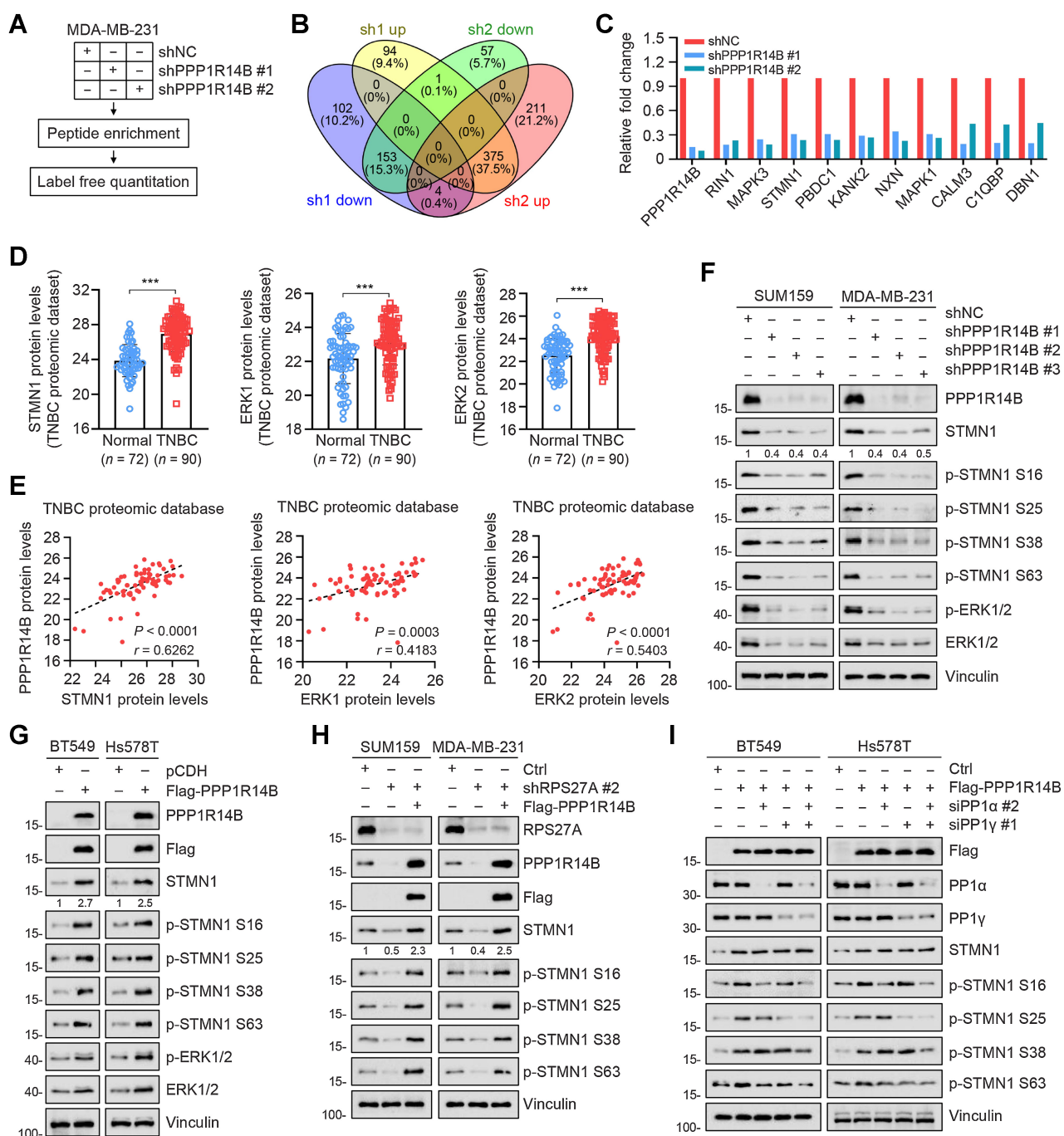
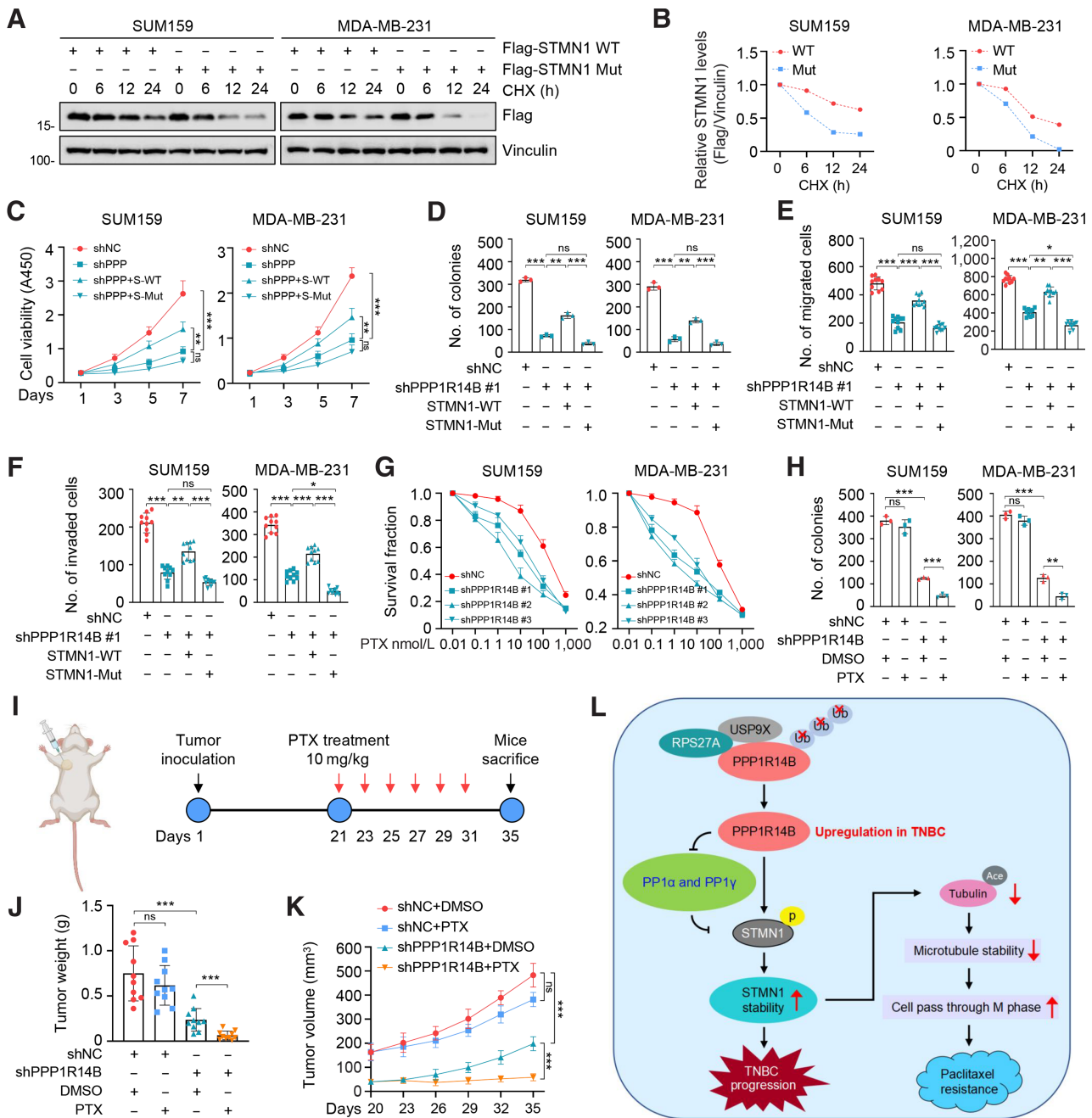


Figure 6.

PPP1R14B regulates phosphorylation and stability of STMN1 partially depending on PPI catalytic subunits  $\alpha$  and  $\gamma$ . **A**, Label-free quantitative proteomic analysis in MDA-MB-231 cell lines stably expressing shNC and shPPP1R14B (#1 and #2). **B**, The number of differentially expressed proteins between cells expressing shNC and shPPP1R14B based on screening by the cutoff value of 1.5-fold change. **C**, The top 10 downregulated proteins in MDA-MB-231 cells with PPP1R14B knockdown. **D**, Protein expression levels of STMN1, ERK1, and ERK2 in 90 TNBC tissues and 72 adjacent normal tissues in the FUSCC-TNBC proteomic database. **E**, Spearman analysis of the correlations of protein expression levels between PPP1R14B and STMN1, ERK1, or ERK2 in the FUSCC-TNBC proteomic database. **F** and **G**, Immunoblotting assays validating the expression levels of downstream proteins in SUM159 and MDA-MB-231 cell lines after PPP1R14B knockdown (**F**), and BT549 and Hs578T cell lines stably overexpressing RPS27A (**G**). **H**, Immunoblotting assays assessing the expression levels of downstream proteins in BT549 and Hs578T cells stably expressing shNC and shRPS27A alone or in combination with or without PPP1R14B overexpression. BT549 and Hs578T cell lines stably expressing sh-RPS27A were infected with lentivirus overexpressing PPP1R14B, and the protein levels were verified using the indicated antibodies. **I**, Immunoblotting images verifying the expression levels of the indicated proteins in BT549 and Hs578T cells stably expressing pCDH and Flag-PPP1R14B alone or in combination transfected with or without siNC, siPP1 $\alpha$  (#2), or siPP1 $\gamma$  (#1). \*\*\*,  $P < 0.001$ .



**Figure 7.**

PPP1R14B accelerates TNBC progression via STMN1 phosphorylation and promotes resistance of TNBC cells to paclitaxel. **A** and **B**, Immunoblotting assays showing the expression levels of STMN1 in SUM159 and MDA-MB-231 cells expressing Flag-STMN1-WT and Flag-STMN1-Mut and treated with DMSO or 100 µg/mL CHX (**A**). Quantitative results of relative STMN1 protein levels (STMN1/Vinculin) are shown in **B**. **C** and **D**, SUM159 and MDA-MB-231 cells stably expressing shNC and shPPP1R14B alone or in combination with Flag-STMN1 (WT or Mut) were subjected to cell proliferation (**C**) and colony formation (**D**) assays. Representative images of survival colonies are shown in Fig. S6D. **E** and **F**, SUM159 and MDA-MB-231 cells stably expressing shNC and shPPP1R14B alone or in combination with Flag-STMN1 (WT or Mut) were subjected to Transwell migration (**E**) and invasion (**F**) assays. Representative images of migrated and invaded cells are shown in Fig. S6E, and corresponding quantitative results are shown in **E** and **F**, respectively. **G**, Cell viability of SUM159 and MDA-MB-231 cells stably expressing shNC and shPPP1R14B (#1, #2, and #3) after treatment with or without increasing doses of paclitaxel (PTX) using the proliferation assay. **H**, Colony formation assays in SUM159 and MDA-MB-231 cells expressing shNC and shPPP1R14B (#1, #2, and #3) were treated with the indicated concentrations of paclitaxel. **I-K**, A total of  $3 \times 10^6$  MDA-MB-231 cells stably expressing shNC and shPPP1R14B were inoculated into the mammary fat pads of 6-week-old BALB/c female nude mice ( $n = 10$ ). After 20 days of injection, DMSO or paclitaxel (10 mg/kg, dissolved in DMSO) was administered by intraperitoneal injection every 2 days and 6 times in total. Images of tumor growth and drug procedure (**I**), tumor weight (**J**), and tumor volume (**K**) are shown. **L**, The proposed working model. \*,  $P < 0.05$ ; \*\*,  $P < 0.01$ ; \*\*\*,  $P < 0.001$ ; ns, no significance. (**I**, Left image was created with BioRender.com.)

chase assays showed that the half-life of mutant STMN1 was substantially shorter than that of wild-type STMN1, suggesting that PPP1R14B enhances STMN1 protein stability via modulating its phosphorylation (Fig. 7A and B). We next examined whether STMN1 phosphorylation is involved in PPP1R14B-induced TNBC progression by ectopic expression WT or mutant STMN1 in PPP1R14B-silenced cells (Supplementary Fig. S6C). Results showed that inhibition of TNBC cell proliferation and colony formation induced by PPP1R14B knockdown was partially rescued by ectopic expression of WT but not mutant STMN1 (Fig. 7C and D; Supplementary S6D). Similarly, Transwell assays revealed that reduced migratory and invasive potential of TNBC cells caused by PPP1R14B depletion was rescued by ectopic expression of WT but not mutant STMN1 (Fig. 7E and F; Supplementary Fig. S6E). Taken together, these results indicate that PPP1R14B exerts oncogenic roles in TNBC progression through, at least in part, regulating phosphorylation and stability of STMN1.

#### **PPP1R14B promotes resistance of TNBC cells to paclitaxel both *in vitro* and *in vivo***

As STMN1 is a microtubule-destabilizing protein and is associated with resistance to microtubule-stabilizing drugs (such as paclitaxel) in various cancers (28), we next examined the impact of PPP1R14B on TNBC cellular sensitivity to paclitaxel. We found that PPP1R14B-depleted cells displayed enhanced sensitivity to paclitaxel as compared with control cells (Fig. 7G). Similar results were obtained from colony formation assays (Fig. 7H; Supplementary Fig. S7A). Furthermore, in mammary fat pad xenograft tumor models, tumor-suppressive effects in mice bearing PPP1R14B-depleted tumors were more pronounced compared with those in control mice following low-dose of paclitaxel administration (Fig. 7I–K; Supplementary Fig. S7B). These results suggest that PPP1R14B contributes to paclitaxel resistance in TNBC cells.

#### **PPP1R14B promotes STMN1-mediated microtubules instability and cell-cycle mitotic progression**

Previous studies revealed that STMN1 regulates acetylation of  $\alpha$ -tubulin (Ace-Tubulin) at lysine 40 (Lys40), thus modulating microtubule stability and contributing to paclitaxel sensitivity (29, 30). To further validate the above results, Ace-Tubulin (Lys40) antibody was used to assess the microtubule stability. Both immunofluorescent and immunoblotting assays showed that depletion of PPP1R14B increased the expression level of Ace-Tubulin (Supplementary Fig. S7C and S7D).

Paclitaxel can stabilize microtubules and arrest the cell cycle of cells in the mitotic phase, thus triggering the apoptosis of cancer cells. Strikingly, cell-cycle analysis demonstrated that depletion of PPP1R14B resulted in an increase of G<sub>2</sub>–M phase cells (Supplementary Fig. S7E). To further distinguish the impact of PPP1R14B on G<sub>2</sub> or M phase of the cell cycle, flow cytometry analysis was performed using the p-H3 S10 antibody to detect mitotic cells. It has been well documented that p-H3 S10 is a specific marker in mitosis and exists only during the late G<sub>2</sub> phase and mitosis (31). Results showed that the percentage of p-H3 S10-positive cells was obviously increased after PPP1R14B knockdown (Supplementary Fig. S7F). Furthermore, immunoblotting assays confirmed this effect using antibodies of cell-cycle markers (Supplementary Fig. S7G). In summary, we conclude that PPP1R14B affects STMN1-mediated microtubule instability and promotes the mitotic progression of the cell cycle.

## **Discussion**

In this study, PPP1R14B was identified as both a tumor promoter and a potential therapeutic target for TNBC. Mechanistically, RPS27A, as an upstream adaptor, recruited USP9X to deubiquitinate PPP1R14B and facilitate upregulation of PPP1R14B in TNBC. PPP1R14B promoted TNBC progression via regulating STMN1 phosphorylation and stability. Moreover, we found that inhibition of PPP1R14B improved tumor sensitivity to anti-paclitaxel therapy (Figs. 7L).

PPP1R14B, a highly conserved member of the PP1 family, has been observed to be dysregulated in several human cancers. For example, recently, LINC00466 was found to function as a sponge to miR-137 to upregulate PPP1R14B, contributing to glioma progression and temozolomide resistance (32). However, the biological function of PPP1R14B and the in-depth molecular mechanisms of PPP1R14B dysregulation in human cancer have not yet been investigated. In this study, we revealed the functional and mechanistic roles of PPP1R14B in TNBC progression and chemoresistance for the first time. Available evidence has shown that PP1 could directly maintain tumor malignancy by targeting Rb, p53, and AKT signaling pathways. In this study, we found that PPP1R14B could function as both a tumor promoter and a potential therapeutic target in TNBC.

Then, we explored the molecular mechanisms underlying the accumulation of PPP1R14B in TNBC. LC-MS/MS analysis implied that RPS27A was one of the interacting proteins of PPP1R14B. RPS27A is a component of the ribosomal 40S subunit and is involved in the encoding of the carboxy terminus of ubiquitin (33). In human cancer, RPS27A interacts with downstream molecules, such as LMP1 and P53, and stabilizes them by suppressing proteasome-mediated ubiquitination to regulate cell-cycle progression (such as G<sub>2</sub>–M phase) and tumor metastasis (33). In this study, we found that PPP1R14B was subjected to proteasome-mediated ubiquitination degradation, and that RPS27A stabilized PPP1R14B through blocking ubiquitination-mediated degradation of PPP1R14B.

Previous studies have shown that there is an interaction of RPS27A with OTUB1 (34) and USP7 (35). These data are consistent with our proteomic results. Consequently, regulation of protein homeostasis by RPS27A through the proteasome-mediated ubiquitination system may partially depend on its interactions with some DUBs. USP9X is one of the most active DUBs (35), and acts as a key DUB for oncoprotein stabilization, such as ALDH1A3 (36), and KDM4C (37). Strikingly, USP9X can function as a tumor promoter or a tumor suppressor, and the complex role of USP9X in human cancers is determined by its various substrates (38). In this study, our results implied that RPS27A acts as an adaptor to recruit USP9X to deubiquitinate PPP1R14B, thus leading to PPP1R14B upregulation in TNBC. However, we cannot rule out the possibility that RPS27A may recruit other deubiquitinases to stabilize PPP1R14B.

PP1 regulatory subunits interact strongly with PP1 catalytic subunits to form the holoenzyme PP1 (5). In fact, the catalytic subunits are responsible for the dephosphorylation reaction, whereas the regulatory subunits can determine the enzyme specificity by alternatively targeting the PP1 holoenzyme to specific subcellular compartments and substrates (39). Therefore, the different functions of PP1 holoenzyme mainly depend on PP1 regulatory subunits and specific substrates. For example, PPP1R10 (also known as PNUTS) forms the PNUTS/PP1c holoenzyme with catalytic subunits PP1 $\alpha$  and PP1 $\gamma$ . On the one hand, PPP1R10 independently accelerates tumor growth and metastasis of TNBC via its alternative splicing lncRNA-PNUTS (40). On the other hand, PNUTS/PP1 $\gamma$  holoenzyme is amplified in human cancers and

PPP1R10 depletion sensitizes resistant breast cancer cells to Aurora inhibition by preventing PP1-dependent dephosphorylation of active Aurora B (41, 42). Meanwhile, PPP1R10 inhibits PP1c-mediated dephosphorylation of Rb in breast cancer (43). In the current study, PPP1R14B was proved to form PP1 holoenzyme by binding with PP1 $\alpha$  and PP1 $\gamma$ . PPP1R14B, as a tumor promoter in TNBC, mediates the phosphorylation of oncoprotein STMN1 through, at least in part, interaction with PP1 $\alpha$  and PP1 $\gamma$ .

STMN1, also known as oncoprotein 18, is involved in the regulation of the microtubule dynamics system. Accumulating evidence shows that STMN1 is highly expressed in multiple types of human cancer, including gastric and colorectal (44), lung (45), and breast (46) cancers, and functions as a tumor promoter contributing to malignant phenotypes. In addition, high expression of STMN1 is associated with chemoresistance, such as paclitaxel (47) and doxorubicin (48). STMN1 has four sites of phosphorylation, including S16, S25, S38, and S63. A growing number of studies identify that phosphorylated STMN1 has similar effects in tumors compared with STMN1 (49). In this study, we observed that PPP1R14B accelerated TNBC progression by regulating STMN1 phosphorylation. PPP1R14B deficiency led to M phase accumulation; thus, its role in paclitaxel sensitivity was explored in this study. The most significant aspect of our finding is that PPP1R14B knockdown obviously improved paclitaxel sensitivity in TNBC by regulating STMN1-mediated microtubule stability. Thus, findings presented here have excellent clinical significance and provide a novel rationale for the future development of antimicrotubule cancer therapeutics for human cancer.

In summary, this study presents significant roles of PPP1R14B in TNBC progression and chemoresistance. The potential mechanism of the PPP1R14B–STMN1–Ace-Tubulin regulatory pattern supports our findings. Moreover, we reveal a detailed mechanism of PPP1R14B accumulation mediated by the RPS27A–USP9X complex in TNBC.

These findings suggest that PPP1R14B may serve as a potential therapeutic target for TNBC.

### Authors' Disclosures

No disclosures were reported.

### Authors' Contributions

**L. Liao:** Software, formal analysis, investigation, methodology, writing—original draft. **Y.-L. Zhang:** Formal analysis, investigation. **L. Deng:** Investigation, methodology. **C. Chen:** Software, validation, methodology. **X.-Y. Ma:** Formal analysis. **L. Andriani:** Validation. **S.-Y. Yang:** Methodology. **S.-Y. Hu:** Software, methodology. **F.-L. Zhang:** Resources, data curation, supervision, funding acquisition, validation. **Z.-M. Shao:** Supervision, project administration. **D.-Q. Li:** Resources, data curation, supervision, funding acquisition, project administration.

### Acknowledgments

The authors are thankful to the TCGA, METABRIC and CPTAC for providing the data analyzed in this study. They are grateful to M.X. Yan and W.J. Chai for helpful suggestions and technical assistance. The work in the Li laboratory is supported, in whole or in part, by the National Natural Science Foundation of China (81572584, 81772805, and 82173275) and the National Key R&D Program of China (2017YFC0908400 and 2018YFE0201600) to D.-Q. Li, and the National Natural Science Foundation of China (82072918 and 82203729) and the Natural Science Foundation of Shanghai (22ZR1413100) to Y.-L. Zhang and F.-L. Zhang.

The publication costs of this article were defrayed in part by the payment of publication fees. Therefore, and solely to indicate this fact, this article is hereby marked “advertisement” in accordance with 18 USC section 1734.

### Note

Supplementary data for this article are available at Cancer Research Online (<http://cancerres.aacrjournals.org/>).

Received August 26, 2022; revised October 22, 2022; accepted December 6, 2022; published first December 9, 2022.

### References

- Sung H, Ferlay J, Siegel RL, Laversanne M, Soerjomataram I, Jemal A, et al. Global cancer statistics 2020: GLOBOCAN estimates of incidence and mortality worldwide for 36 cancers in 185 countries. *CA Cancer J Clin* 2021;71:209–49.
- Garrido-Castro AC, Lin NU, Polyak K. Insights into molecular classifications of triple-negative breast cancer: improving patient selection for treatment. *Cancer Discov* 2019;9:176–98.
- Schmid P, Abraham J, Chan S, Wheatley D, Brunt AM, Nemsadze G, et al. Capivasertib plus paclitaxel versus placebo plus paclitaxel as first-line therapy for metastatic triple-negative breast cancer: the PAKT trial. *J Clin Oncol* 2020;38:423–33.
- Shi Y. Serine/threonine phosphatases: mechanism through structure. *Cell* 2009;139:468–84.
- Felgueiras J, Jeronimo C, Fardilha M. Protein phosphatase 1 in tumorigenesis: is it worth a closer look? *Biochim Biophys Acta Rev Cancer* 2020;1874:188433.
- Wurzenberger C, Gerlich DW. Phosphatases: providing safe passage through mitotic exit. *Nat Rev Mol Cell Biol* 2011;12:469–82.
- Chen MJ, Dixon JE, Manning G. Genomics and evolution of protein phosphatases. *Sci Signal* 2017;10:eaag1796.
- Smith I, Robertson J, Kilburn L, Wilcox M, Evans A, Holcombe C, et al. Long-term outcome and prognostic value of Ki67 after perioperative endocrine therapy in postmenopausal women with hormone-sensitive early breast cancer (POETIC): an open-label, multicentre, parallel-group, randomised, phase 3 trial. *Lancet Oncol* 2020;21:1443–54.
- Krzyzosiak A, Sigurdardottir A, Luh L, Carrara M, Das I, Schneider K, et al. Target-based discovery of an inhibitor of the regulatory phosphatase PPP1R15B. *Cell* 2018;174:1216–28.
- Eto M, Karginov A, Brautigan DL. A novel phosphoprotein inhibitor of protein type-1 phosphatase holoenzymes. *Biochemistry* 1999;38:16952–7.
- Elfring LK, Axton JM, Fenger DD, Page AW, Carminati JL, Orr-Weaver TL. Drosophila PLUTONIUM protein is a specialized cell cycle regulator required at the onset of embryogenesis. *Mol Biol Cell* 1997;8:583–93.
- Worley MJ Jr, Liu S, Hua Y, Kwok JS, Samuel A, Hou L, et al. Molecular changes in endometriosis-associated ovarian clear cell carcinoma. *Eur J Cancer* 2015;51:1831–42.
- Xiang N, Chen T, Zhao X, Zhao M. In vitro assessment of roles of PPP1R14B in cervical and endometrial cancer. *Tissue Cell* 2022;77:101845.
- Wang R, Wu Y, Yu J, Yang G, Yi H, Xu B, et al. Plasma messenger RNAs identified through bioinformatics analysis are novel, non-invasive prostate cancer biomarkers. *Onco Targets Ther* 2020;13:541–8.
- Deng M, Peng L, Li J, Liu X, Xia X, Li G, et al. PPP1R14B is a prognostic and immunological biomarker in pan-cancer. *Front Genet* 2021;12:763561.
- Mosquera Orgueira A, Antelo Rodriguez B, Diaz Arias JA, Diaz Varela N, Bello Lopez JL. A three-gene expression signature identifies a cluster of patients with short survival in chronic lymphocytic leukemia. *J Oncol* 2019;2019:9453539.
- Young L, Sung J, Stacey G, Masters JR. Detection of mycoplasma in cell cultures. *Nat Protoc* 2010;5:929–34.
- Sun R, Xie H-Y, Qian J-X, Huang Y-N, Yang F, Zhang F-L, et al. FBXO22 possesses both protumorigenic and antimetastatic roles in breast cancer progression. *Cancer Res* 2018;78:5274–86.
- Gong T-Q, Jiang Y-Z, Shao C, Peng W-T, Liu M-W, Li D-Q, et al. Proteome-centric cross-omics characterization and integrated network analyses of triple-negative breast cancer. *Cell Rep* 2022;38:110460.
- Jiang Y-Z, Ma D, Suo C, Shi J, Xue M, Hu X, et al. Genomic and transcriptomic landscape of triple-negative breast cancers: subtypes and treatment strategies. *Cancer Cell* 2019;35:428–40.
- Yang Y-L, Zhang Y, Li D-D, Zhang F-L, Liu H-Y, Liao X-H, et al. RNF144A functions as a tumor suppressor in breast cancer through ubiquitin ligase

- activity-dependent regulation of stability and oncogenic functions of HSPA2. *Cell Death Differ* 2020;27:1105–18.
22. Lu Q, Lu D, Shao Z-M, Li D-Q. Deubiquitinase ubiquitin-specific protease 9X regulates the stability and function of E3 ubiquitin ligase ring finger protein 115 in breast cancer cells. *Cancer Sci* 2019;110:1268–78.
  23. Jia X, Chen J, Megger DA, Zhang X, Kozlowski M, Zhang L, et al. Label-free proteomic analysis of exosomes derived from inducible hepatitis B virus-replicating HepAD38 cell line. *Mol Cell Proteomics* 2017;16:S144–S60.
  24. Zhang T-M, Liao L, Yang S-Y, Huang M-Y, Zhang Y-L, Deng L, et al. TOLLIP-mediated autophagic degradation pathway links the VCP-TMEM63A-DERL1 signaling axis to triple-negative breast cancer progression. *Autophagy* 2022;1–17. doi: 10.1080/15548627.2022.2103992.
  25. Hong SW, Kim SM, Jin DH, Kim YS, Hur DY. RPS27a enhances EBV-encoded LMP1-mediated proliferation and invasion by stabilizing of LMP1. *Biochem Biophys Res Commun* 2017;491:303–9.
  26. Carafa V, Nebbioso A, Cuomo F, Rotili D, Cobellis G, Bontempo P, et al. RIP1-HAT1-SIRT complex identification and targeting in treatment and prevention of cancer. *Clin Cancer Res* 2018;24:2886–900.
  27. Larsson N, Melander H, Marklund U, Osterman O, Gullberg M. G<sub>2</sub>-M transition requires multisite phosphorylation of oncoprotein 18 by two distinct protein kinase systems. *J Biol Chem* 1995;270:14175–83.
  28. Balachandran R, Welsh MJ, Day BW. Altered levels and regulation of stathmin in paclitaxel-resistant ovarian cancer cells. *Oncogene* 2003;22:8924–30.
  29. Liu X-Y, Jiang W, Ma D, Ge L-P, Yang Y-S, Gou Z-C, et al. SYTL4 downregulates microtubule stability and confers paclitaxel resistance in triple-negative breast cancer. *Theranostics* 2020;10:10940–56.
  30. Pan Z, Fang Q, Li L, Zhang Y, Xu T, Liu Y, et al. HN1 promotes tumor growth and metastasis of anaplastic thyroid carcinoma by interacting with STMN1. *Cancer Lett* 2021;501:31–42.
  31. Laflamme P, Mansoori BK, Sazanova O, Orain M, Couture C, Simard S, et al. Phospho-histone-H3 immunostaining for pulmonary carcinoids: impact on clinical appraisal, interobserver correlation, and diagnostic processing efficiency. *Hum Pathol* 2020;106:74–81.
  32. Zhao M, Shao Y, Xu J, Zhang B, Li C, Gong J. LINC00466 impacts cell proliferation, metastasis and sensitivity to temozolomide of glioma by sponging miR-137 to regulate PPP1R14B expression. *Onco Targets Ther* 2021;14:1147–59.
  33. Li H, Zhang H, Huang G, Bing Z, Xu D, Liu J, et al. Loss of RPS27a expression regulates the cell cycle, apoptosis, and proliferation via the RPL11-MDM2-p53 pathway in lung adenocarcinoma cells. *J Exp Clin Cancer Res* 2022;41:33.
  34. Zhang W, Qiu W. OTUB1 recruits tumor infiltrating lymphocytes and is a prognostic marker in digestive cancers. *Front Mol Biosci* 2020;7:212.
  35. Grou CP, Pinto MP, Mendes AV, Domingues P, Azevedo JE. The de novo synthesis of ubiquitin: identification of deubiquitinases acting on ubiquitin precursors. *Sci Rep* 2015;5:12836.
  36. Chen Z, Wang H-W, Wang S, Fan L, Feng S, Cai X, et al. USP9X deubiquitinates ALDH1A3 and maintains mesenchymal identity in glioblastoma stem cells. *J Clin Invest* 2019;129:2043–55.
  37. Jie X, Fong WP, Zhou R, Zhao Y, Meng R, et al. USP9X-mediated KDM4C deubiquitination promotes lung cancer radioresistance by epigenetically inducing TGF- $\beta$ 2 transcription. *Cell Death Differ* 2021;28:2095–111.
  38. Lu Q, Zhang F-L, Lu D-Y, Shao Z-M, Li D-Q. USP9X stabilizes BRCA1 and confers resistance to DNA-damaging agents in human cancer cells. *Cancer Med* 2019;8:6730–40.
  39. Casamayor A, Arino J. Controlling Ser/Thr protein phosphatase PP1 activity and function through interaction with regulatory subunits. *Adv Protein Chem Struct Biol* 2020;122:231–88.
  40. Grelet S, Link LA, Howley B, Obellianne C, Palanisamy V, Gangaraju VK, et al. A regulated PNUMS mRNA to lncRNA splice switch mediates EMT and tumour progression. *Nat Cell Biol* 2017;19:1105–15.
  41. Dingar D, Tu WB, Reseta D, Lourenco C, Tamachi A, De Melo J, et al. MYC dephosphorylation by the PP1/PNUMS phosphatase complex regulates chromatin binding and protein stability. *Nat Commun* 2018;9:3502.
  42. Wang F, Wang L, Fisher LA, Li C, Wang W, Peng A, et al. Phosphatase 1 nuclear targeting subunit (PNUMS) regulates aurora kinases and mitotic progression. *Mol Cancer Res* 2019;17:10–9.
  43. Choy MS, Hieke M, Kumar GS, Lewis GR, Gonzalez-DeWhitt KR, Kessler RP, et al. Understanding the antagonism of retinoblastoma protein dephosphorylation by PNUMS provides insights into the PP1 regulatory code. *Proc Natl Acad Sci U S A* 2014;111:4097–102.
  44. Liu J, Li J, Wang K, Liu H, Sun J, Zhao X, et al. Aberrantly high activation of a FoxM1-STMN1 axis contributes to progression and tumorigenesis in FoxM1-driven cancers. *Signal Transduct Target Ther* 2021;6:42.
  45. Bao P, Yokobori T, Altan B, Iijima M, Azuma Y, Onozato R, et al. High STMN1 expression is associated with cancer progression and chemoresistance in lung squamous cell carcinoma. *Ann Surg Oncol* 2017;24:4017–24.
  46. Kuang X-Y, Jiang H-S, Li K, Zheng Y-Z, Liu Y-R, Qiao F, et al. The phosphorylation-specific association of STMN1 with GRP78 promotes breast cancer metastasis. *Cancer Lett* 2016;377:87–96.
  47. Xun G, Hu W, Li B. PTEN loss promotes oncogenic function of STMN1 via PI3K/AKT pathway in lung cancer. *Sci Rep* 2021;11:14318.
  48. Li Y, Liang Y, Sang Y, Song X, Zhang H, Liu Y, et al. MiR-770 suppresses the chemo-resistance and metastasis of triple negative breast cancer via direct targeting of STMN1. *Cell Death Dis* 2018;9:14.
  49. Magron A, Elowe S, Carreau M. The fanconi anemia C protein binds to and regulates Stathmin-1 phosphorylation. *PLoS One* 2015;10:e0140612.